Interactions between Rain and Wind Waves

YING-KEUNG POON, SHIH TANG, AND JIN WU

Air–Sea Interaction Laboratory, Graduate College of Marine Studies, University of Delaware, Lewes, Delaware

(Manuscript received 5 July 1991, in final form 24 September 1991)

ABSTRACT

Effects of rain on surface waves have been investigated in a circulating wind-wave tank. Surface displacement and slope spectra under different wind velocities were measured near the upwind and downwind edges of a region with simulated rains. Spatially uniform rains of varied intensities with drop size of about 2.6 mm and spacing of 3 cm were used. Damping of surface waves by rain was observed in the frequency region of 2–5 Hz, and there was an increase in the damping rate with rain intensity. The effective eddy viscosity in the rain-induced mixed layer was found to be an order of magnitude greater than the molecular viscosity of water. As for rain-induced ripples, spectral densities of the surface slope in the frequency range of 10–100 Hz increased with the rain intensity. However, at the highest wind velocity (6.34 m s^{-1}) of the present experiment, the ripple structure was influenced primarily by wind, with rain introducing no observable effects.

1. Introduction

Rain falling over the ocean can change the structure of surface waves in many ways. When raindrops strike the water surface, they generate ripples (Houk and Green 1976). Meanwhile, the rain can enhance the wind stress acting on the sea surface (Caldwell and Elliott 1972) and hence affect surface waves. Eddies generated at the rain-induced mixed layer immediately below the air–water interface (Katsaros and Beuttner 1969; Green and Houk 1979) may also affect wave structures through wave–turbulence interaction (Wang and Chern 1988).

Effects of rain on the sea surface have only been scarcely studied and were mostly confined to the interaction between a single raindrop and water body (Kilgore and Day 1963; Chapman and Critchlow 1967; Siscoe and Levin 1971). Rain was suggested much earlier to have a calming effect on surface gravity waves (Reynolds 1900). Recently, an enhanced damping of monochromatic mechanical waves passing a region of simulated rains was observed by Tsimplis and Thorpe (1989); the effective eddy viscosity causing the additional damping was also found to be an order of magnitude greater than the molecular viscosity of water. Based on the momentum exchange between rain and surface waves, Le Mèhautè and Khangaonkar (1990) found that for an intense rain the damping rate depends on rain intensity, terminal velocity, and inclination of the drops. In addition to the damping of gravity waves, rain also generates ripples (Houk and Green 1976); their measurements, however, were limited to low-frequency wave components (<10 Hz). Le Mèhautè (1988) also found analytically that ripples generated by spherical water drops entering a quiescent water body were in a rather narrow wavenumber range around 1.43 rad cm^{-1}, corresponding to the minimum possible group velocity.

Both the attenuation of surface waves and generation of ripples by rain are simultaneously measured in the present experiment under different wind and rain conditions. The attenuation is examined by evaluating changes in the frequency spectra of surface displacements. The ripples are best quantified in terms of their slopes; the latter are measured with a laser-optic system. Relative importance between rain- and wind-generated ripples is evaluated, which is also helpful in understanding radar backscattering from the sea surface under rain.

2. Experiments

a. Facility

1) CIRCULATING WIND-WAVE TANK

All experiments are carried out in an oval-shaped circulating wind-wave tank (see Fig. 1). The tank consists of two straight sections, each 7 m long; they are connected by two semicircular sections with the centerline radius of 1.35 m. The tank is 31 cm wide and 44.5 cm high; the water depth is maintained at 24 cm. A variable-speed fan is mounted in the back straight section of the tank. Horizontal guiding vanes are installed in front of the fan to regulate airflows. Vertical guiding vanes are installed in the semicircular sections

Corresponding author address: Dr. Ying-Kueng Poon, University of Delaware, Air–Sea Interaction Laboratory, Graduate College of Marine Studies, Lewes, DE 11959.

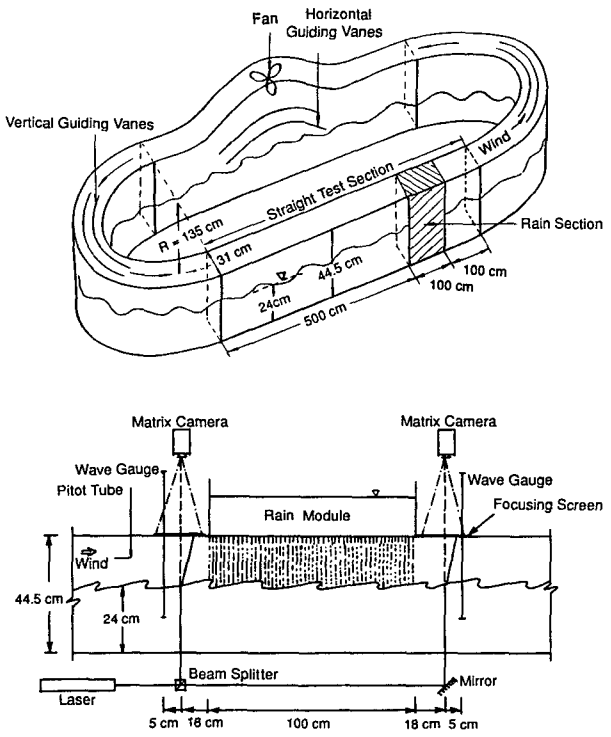

FIG. 1. Circulating wind-wave tank and experimental setup.

to minimize secondary flows in both the air and water. Artificial rain is simulated over a 1-m stretch of the front straight section of the tank; the upwind end of the rain region is 5 m downwind from the end of the curve section. Filtered tap water is used for all the experiments.

2) ARTIFICIAL RAIN SIMULATOR

A rain module similar to those of Katsaros and Beuttner (1969) and Green and Houk (1979) is used. Spanning across the tank, the module is a rectangular box 1 m long and 20 cm high. Uniformly spaced hypodermic needles, 3 cm apart from center to center, are arranged in a staggered fashion at the bottom of the box. The rain intensity is controlled by the water head above needle tips. Needles of gauge number 23 are used to generate raindrops about 2.6 mm in diameter; the latter is determined by measuring the weight of drops, assuming that they are spherical. For our simulated rain conditions, the drop diameter depends only on the needle size but not the water head. Calibration of the drop size is done without wind, and the effect of wind on the drop size is not considered. According to Cataneo and Stout (1968) and Willis and Tattelman (1989), over a wide range of rain intensities from 2 to over 250 mm h^{-1}, the drop diameters are within 0.5 to 5 mm. Hence, the drop size chosen in the present experiment is found in natural rain.

b. Measurements

As shown in Fig. 1, surface displacements are measured with two capacitance-type wave probes, placed at a distance 23 cm upwind and downwind away from the rain section, respectively. Each probe consists of a 0.5-mm diameter Tantalum wire with an oxidized coating and a controlling circuit. The surface slope is measured with a laser-optic system, which utilizes the light-refraction principle (Haimbach 1985). A laser beam directed vertically upward is refracted at the water surface to project an image on a horizontal focusing screen, which is also a part of the tank cover. A matrix camera with 100 × 100 photodiodes is used to track the image of the beam. From the displacement of the image from its neutral position corresponding to a still water surface, and the distance between the screen and the still water surface, both the upwind–downwind and crosswind slopes can be deduced from Snell's law. With the present setup, the resolution of the slopes is 15 mrad. Measurements of surface slopes are performed at a distance of 18 cm away from either edge of the rain section. The measurement locations for surface displacements and slopes are chosen such that they are not directly disturbed by rain but are as close as possible to the edges of the rain section. Due to the wind, the maximum horizontal travel distance of raindrops before reaching the water surface is about 10 cm under the highest wind velocity. This observed displacement agrees with a simple numerical simulation on the trajectories of spherical drops, to be discussed fully in section 4a.

The experiments are conducted with wind velocities of 3.41, 4.88, and 6.34 m s^{-1} measured 11 cm above the mean water surface. The rain intensities are 35, 65, and 100 mm h^{-1}. Before the rain is introduced, the wind is turned on for about 30 minutes; it is measured with a Pitot tube about 40 cm upwind of the rain section. Surface displacements and slopes are also measured at specified locations as discussed earlier. After the rain is introduced, measurements of surface displacements and slopes are again taken at those locations for the rain intensity of 100 mm h^{-1} as a reference. Measurements of surface displacements and slopes at other rain intensities are then taken only at the downwind side. For each condition, the displacement data are recorded for a period of 409.6 s at the sampling rate of 20 Hz; and the slope data for a period of 163.84 s at the rate of 400 Hz.

3. Results

a. The damping of surface waves

The damping of surface waves is evaluated from frequency spectra of surface displacements measured at the downwind side of the rain region. We report here only the results measured at the two highest wind velocities, and leave the discussion for the lowest wind velocity of 3.41 m s^{-1} with very small surface displace-

ments to surface slopes for section 4. Due to the growth of wind waves, the root-mean-square (rms) surface displacement obtained from measurements at the upwind and downwind sides of the rain section are different even without the rain. At the wind velocity of 4.88 m s^{-1}, the rms surface displacement at the downwind side is about 4% greater than that at the upwind side; the corresponding increase is about 3% at 6.34 m s^{-1}. Hence, only the measurements obtained at the downwind side are used to examine changes in the surface displacement due to the presence of rain. In other words, we compare measured surface displacements with rain to those without rain at the same location.

Each set of 409.6-s surface displacement data is divided into 32 segments; this gives a frequency resolution of 0.078 Hz. Each data segment is windowed (Blackman and Tukey 1959), and the spectrum for each segment is calculated with the standard fast Fourier transform. The lost variance due to windowing is corrected, and the final spectrum is obtained from the average of all 32 corrected segments. The results are shown in Fig. 2, where $E(f)$ is the spectral density of displacements with f being the frequency. It can be seen that without rain, $E(f)$ for wind velocity of 4.88 m s^{-1} (Fig. 2a) shows an f^{-n} dependence, where n is between 3 and 4 in the range of $3 < f < 5$ Hz and gradually increases to 4 towards higher frequencies of $f > 5$ Hz. The f^{-4} dependence for the high-frequency range agrees well with the spectra suggested by Toba (1973) and Phillips (1985). For wind velocity of 6.34 m s^{-1} (Fig. 2b), the exponent of the frequency dependence at the frequency range of 3–5 Hz has a value smaller than 4, and the exponent n does not increase at higher frequencies. This is possibly due to a greater effect of the Doppler shift at higher winds (Wright and Keller 1971; Shemdin 1972; Wu 1975; Banner 1990).

Contributions to the Doppler shift of wave frequencies are from both orbital motions of waves and wind-induced drift currents. Recently, Banner (1990) examined the effect of dominant-wave steepness, $A_p k_p$, on the shape of the frequency spectrum, where A_p and k_p are, respectively, the amplitude and wavenumber at the spectral peak. The amplitude A_p is estimated from the displacement spectrum integrated over the frequency range of 0.5–1.5 f_p, where f_p is the frequency at the spectral peak. The results show that for $f/f_p > 3$, the Doppler shift increases the exponent of the frequency dependence, and the magnitude of change increases with A_p. For wind velocities of 4.88 and 6.34 m s^{-1} in the present study, $A_p k_p$ are, respectively, 0.09 and 0.12, and f_p are 2.6 and 2.1 Hz. Therefore, the dominant-wave steepness should affect the portion of frequency spectra with frequencies higher than 7.8 and 6.3 Hz for wind velocities of 4.88 and 6.34 m s^{-1}, respectively. In addition, there is a greater effect at higher winds because A_p is larger. This explains partially the gentler slope at the high-frequency range of the displacement spectrum at higher winds. In addition, the contribution of wind-induced drifts to the Doppler shift

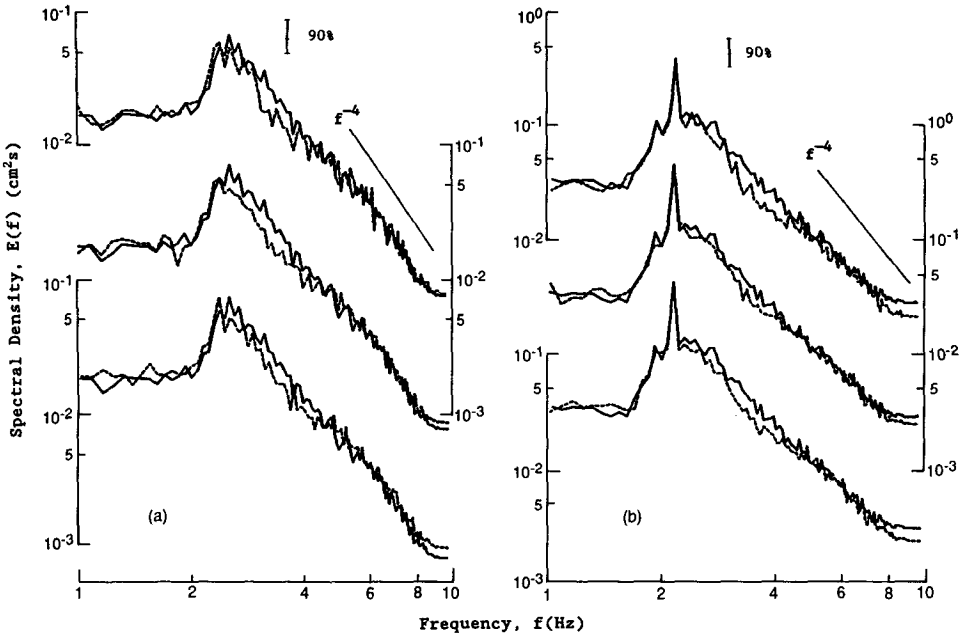

FIG. 2. Comparisons of displacement spectra measured with and without rain. The wind velocities are (a) 4.88 and (b) 6.34 m s^{-1}, respectively. The results from top to bottom are obtained at rain intensities of 100, 65, and 35 mm h^{-1}, respectively; results measured without rain are shown as solid lines and those with rain as dashed lines.

is also greater for higher winds. Wu (1975) showed that for wave frequencies smaller than about 8 Hz, there is an increase in the Doppler shift with wave frequency and the magnitude of shift increases with the surface-drift current.

Frequency spectra of displacements with and without rain at the wind velocity of 4.88 m s^{-1} are compared in Fig. 2a. With the presence of rain, the shapes of the spectra are not affected, except that there are decreases in the wave energy at frequencies between that at the spectral peak and 5 Hz. Similar results are found at the wind velocity of 6.34 m s^{-1} as shown in Fig. 2b. To better demonstrate the damping effect, we examine the spatial damping rate of waves due to presence of rain. For monochromatic waves, the damping coefficient, Δ, is usually defined as

$$A = A_0 e^{-\Delta L}, \quad (1)$$

where A_0 and A are the wave amplitudes at a distance of L apart. For the present study, we are dealing with wind waves and are interested in examining the damping for each frequency component,

$$E^{1/2}(f) = E_0^{1/2}(f) e^{-\Delta(f)L}, \quad (2)$$

in which $E(f)$ and $E_0(f)$ are, respectively, the spectral densities of displacements measured at the downwind edge of the rain region with and without rain, and L is 1 m. Since measurements at the same location are being compared, the calculated $\Delta(f)$ from Eq. (2) is solely due to the presence of rain. The results are shown in Fig. 3. Despite the scatter of data, we can still see from Fig. 3a that for the wind velocity of 4.88 m s^{-1}, most of the damping occurs at a narrow range of frequency between 2.3 and 4.5 Hz, and the maximum damping occurs near 3.1 Hz. For the wind velocity of 6.34 m s^{-1}, damping occurs mainly between 2 and 5 Hz, and the maximum damping at about 3.5 Hz. As discussed earlier, these differences are probably caused by the difference in the frequency shift at two wind velocities. Wu (1975) proposed an empirical relation between the measured and intrinsic phase velocities, wave frequency, and drift currents. Based on his results and the surface drifts measured in the same tank by Wang and Wu (1987) under similar conditions, it is estimated that after corrections for the Doppler shift, the frequency at which the maximum wave damping occurs at both wind velocities is about 2.8 Hz, corresponding to the wavelength of about 20 cm. The dependence of the damping rate on the rain intensity will be discussed later.

b. *The generation of surface ripples*

Similar to the displacement data, the 163.84-s upwind–downwind slope data are divided into 16 segments, each consisting of 4096 data points. The final slope spectra shown in Fig. 4 are then obtained from

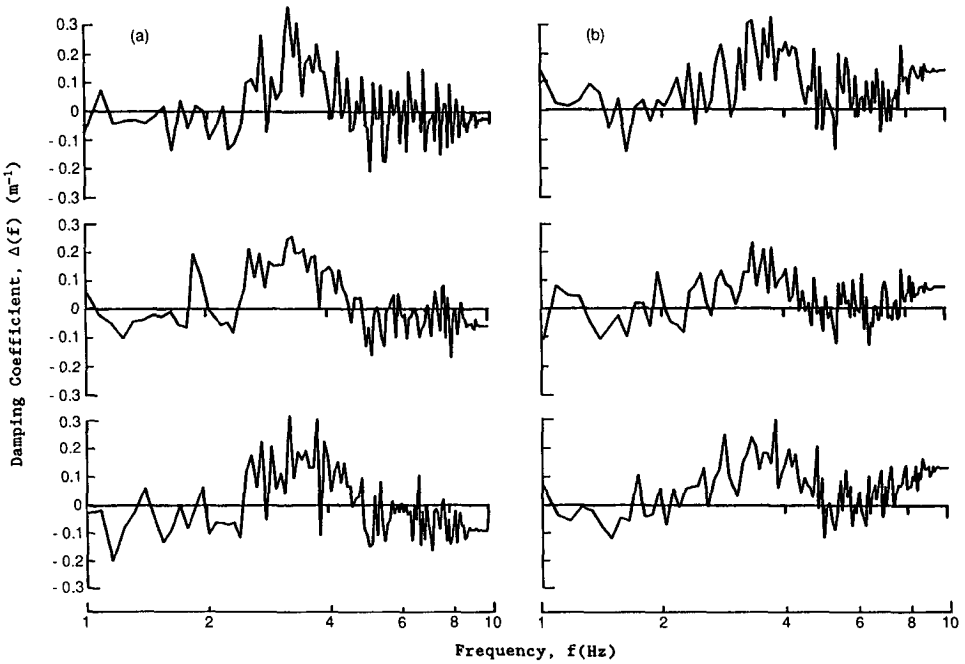

FIG. 3. Damping coefficients $\Delta(f)$ at various frequencies. The wind velocities are (a) 4.88 and (b) 6.34 m s^{-1}, respectively; the results from top to bottom are obtained at rain intensities of 100, 65, and 35 mm h^{-1}, respectively.

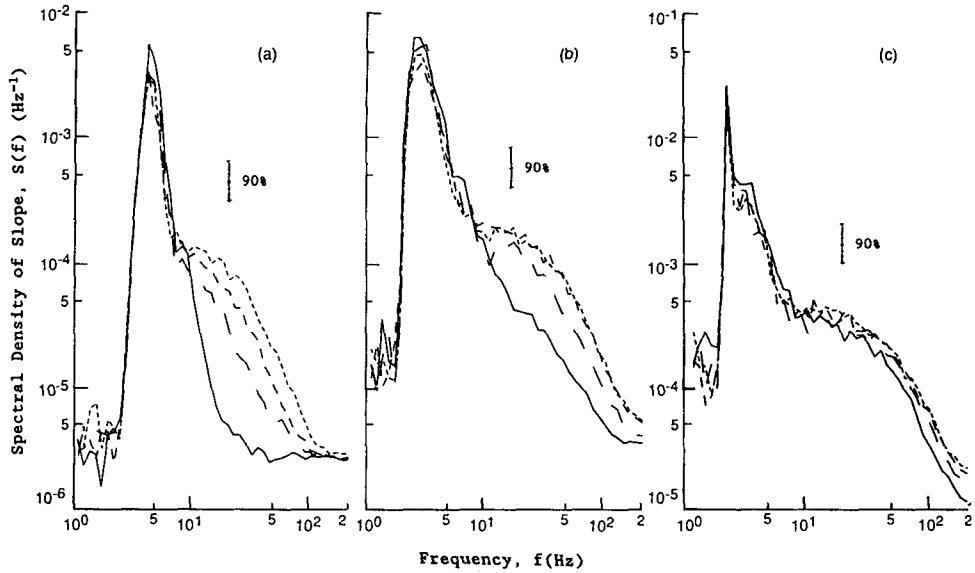

FIG. 4. Measured upwind–downwind slope spectra with and without rain. Measurements are taken at wind velocities of (a) 3.41, (b) 4.88, and (c) 6.34 m s^{-1}, respectively; the results are obtained without rain (solid line) and with rain intensities of 35 (long dashed line), 65 (medium dashed line), and 100 mm h^{-1} (short dashed line), respectively.

frequency smoothing and segment averaging. Without rain, the spectral densities are seen to increase with the wind velocity. In addition, the frequency of spectral peak decreases as the wind velocity increases, indicating that dominant waves become longer. The shape of slope spectra first shows a steep decrease of the spectral density at frequencies just greater than the peak frequency and is followed by a gentler decrease, as in previous laboratory measurements by Long and Huang (1976) and Haimbach (1985). For wind velocities of 4.88 and 6.34 m s^{-1}, the spectral peaks occur, respectively, at frequencies of 2.8 and 2.1 Hz, close to those of the displacement spectra at 2.6 and 2.1 Hz.

The presence of rain is seen to change significantly the slope spectra, especially at low winds. For frequencies higher than about 10 Hz, there is an increase in the spectral density with the rain intensity. At the highest wind velocity of 6.34 m s^{-1}, the changes of slope spectra with the presence of rain are much less significant than those at two lower wind conditions; the ripple structures under the highest wind are dominated by the wind action. To better illustrate the generation of ripples by rain, the ratio between the difference of spectral densities with and without rain and the spectral density without rain, $(S - S_0)/S_0$, is plotted in Fig. 5. The spectral density at the lowest wind velocity and heaviest rain condition is seen raised up to 20 times of those without rain. With the increasing wind velocity, the effect of rain is seen clearly in the figure to be less important. In general, it is found that the rain generates ripples of frequencies between 10 and 100 Hz.

4. Discussion

a. Effects of rain conditions on wave damping

Wave damping by rain was studied by Tsimplis and Thorpe (1989) under very different rain conditions. Monochromatic mechanical waves with frequencies between 1.8 and 4.2 Hz were generated at one end of a straight tank and propagated through a rain region 2 m long. The rain drop was 3.2 mm in diameter, and the rain intensity was 600 mm h^{-1}. The damping coefficients were calculated by them according to Eq. (1) with corrections for damping due to side walls and bottom of the tank; their results are reproduced in Fig. 6. In the figure, the mean values of $\Delta(f)$ obtained in the present experiment at wind velocities of 4.88 and 6.34 m s^{-1} with the same rain intensity are also presented. Our measurements showed that rain has no effect on the waves in the area before the rain section. Since it is unlikely that rain will affect damping due to the side walls and our results are obtained from measurements at the same location, no corrections on the calculated damping coefficients are performed.

It can be seen from Fig. 6 that the damping coefficients obtained by Tsimplis and Thorpe are generally greater than those obtained in the present study. Both groups of results indicate that the waves with frequencies lower than 2 Hz are not affected by the rain. For $2 < f < 3.5$ Hz, both results are again compared fairly well, indicating a gradual increase of the wave damping with frequency. For $3.5 < f < 4.2$ Hz, Tsimplis and

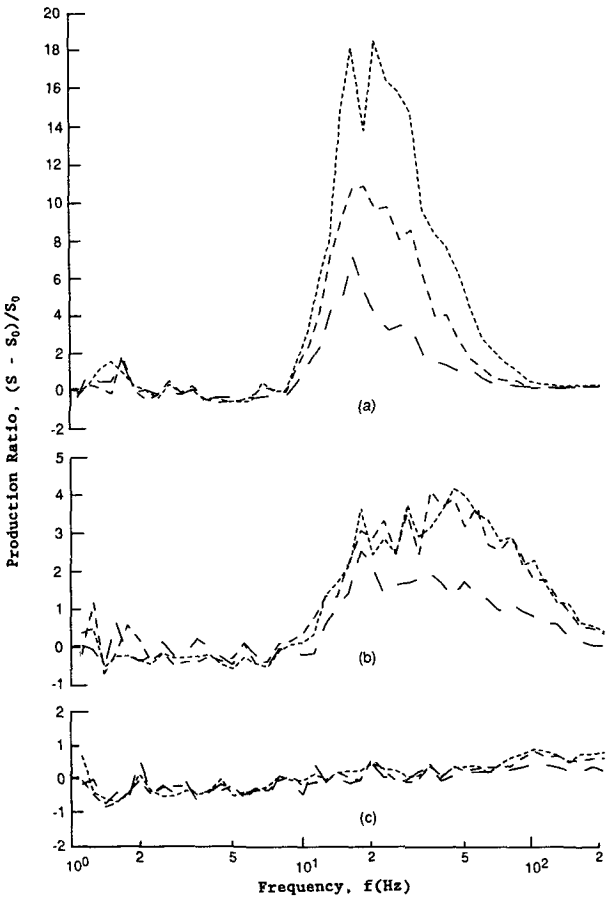

FIG. 5. Production ratios of rain-generated to wind-generated ripples. Measurements are taken at wind velocities of (a) 3.41, (b) 4.88, and (c) 6.34 m s^{-1}, respectively; the production ratios are obtained for rain intensities of 35 (long dashed line), 65 (medium dashed line), and 100 mm h^{-1} (short dashed line), respectively.

Thorpe's results show a rapid increase of the wave damping with frequency, while the present results show a slight decrease in the damping coefficient. This difference is possibly due to the differences in experimental conditions. Our study is on the interaction between rain and wind waves; the rain-generated ripples are convected downstream by the wind-induced current and long waves. Consequently, in addition to the damping of wind waves due to the rain, the waves generated by rain are also present at the downwind section. Although the Stokes drift is also present in wind waves, its magnitude is small in comparison to the wind-induced drift (Wu 1975). In Tsimplis and Thorpe's experiment, there is no wind-induced current, only the Stokes drift. The rain-generated ripples were not convected downstream fast enough and were damped by the time they reached the downwind location through viscous dissipation.

Since rain-generated ripples are always present, the present study represents a more realistic situation than that of Tsimplis and Thorpe (1989). Although the surface displacements are measured outside the simulated rain regions in both studies with the presence of wind-induced currents, some of the rain-generated ripples are included in the present study but not in Tsimplis and Thorpe's measurements. Moreover, in addition to wind stress, rain-induced surface stress is present with the wind; the latter can also affect the surface waves. In the field raindrops are moving at the same velocity as the wind at a height far above the sea surface. As the drops fall, they are retarded by the wind since the wind velocity decreases toward the sea surface. Raindrops were estimated by Caldwell and Elliott (1971) to maintain about 85% of their original horizontal velocity when they reach the sea surface; this contributes to a rain-induced surface stress. The latter was found to be comparable to the wind stress at low winds (several meters per second) and moderate to heavy rain conditions (several centimeters per hour). In our laboratory study, it is quite the contrary, as raindrops are initially at rest and they gain their horizontal momentum from the wind while they are falling. The contribution of rain-induced stress at the water surface for our experiments is then estimated.

Assuming the raindrops are spherical, the equations of motion of a single drop can be written as

$$\frac{du}{dt} = \frac{3}{4}\frac{\rho_a}{\rho}\frac{C_d}{d}U_r(U_a - u)$$

$$\frac{dw}{dt} = g - \frac{3}{4}\frac{\rho_a}{\rho}\frac{C_d}{d}U_r w, \qquad (3)$$

where u and w are, respectively, the horizontal and vertical (positive downward) velocities; t is time; ρ_a and ρ are the density of air and water, respectively; d is the drop diameter; C_d is the drag coefficient; g is the gravitational acceleration; U_a is the wind velocity; and U_r is the speed of the drop relative to air

$$U_r = [(U_a - u)^2 + w^2]^{1/2}; \qquad (4)$$

C_d varies with the Reynolds number $\mathrm{Re} = U_r d/\nu_a$, where ν_a is the kinematic viscosity of air. In our simulation, the values of C_d are calculated from the equations suggested by Raudkivi (1976), and the wind velocity U_a is based on the wind profile measured upstream of the rain section. For wind velocities of 4.88 and 6.34 m s^{-1}, the maximum horizontal displacements of raindrops are found to be, respectively, 7.8 and 11.8 cm, agreeing well with our visual observations. Upon arriving at the water surface, the vertical velocity of the rain drops is 1.9 m s^{-1} regardless of the wind velocities. The horizontal velocities, however, are 0.7 and 1.0 m s^{-1}, corresponding to about 14% and 17% of the wind velocities at 4.88 and 6.34 m s^{-1}, respectively. The ratio of the horizontal velocity of raindrops to that of the wind is smaller in laboratory than in field

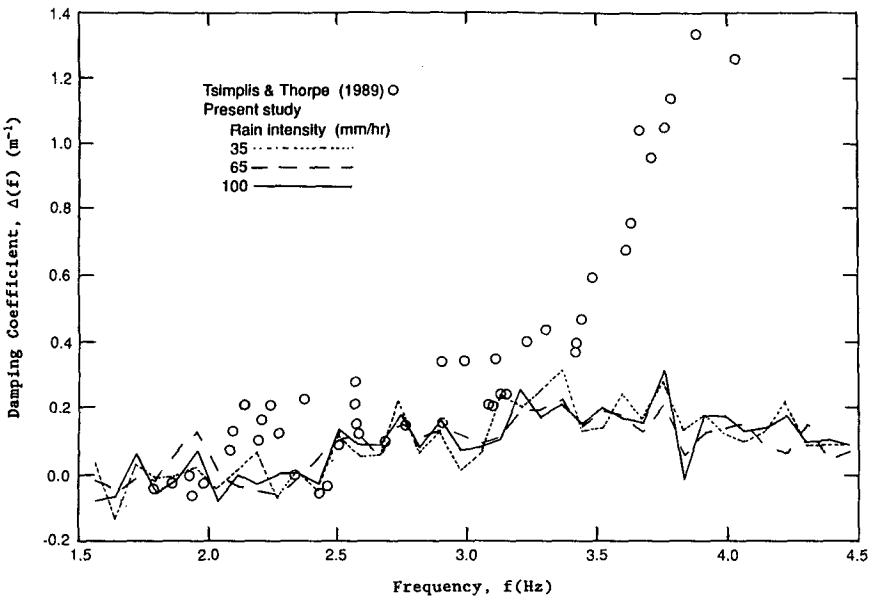

FIG. 6. Comparisons of damping coefficients obtained by Tsimplis and Thorpe (1989) and this study.

conditions. However, since the vertical velocities of raindrops are also reduced, the drops strike the water surface at an angle of 20°–30°, similar to those in the field.

The horizontal stress induced by rain, τ_r, can be calculated from $\tau_r = \rho UI$, where U is the horizontal velocity of raindrops just before entering the water and I is the rain intensity. It is found that the ratio between the rain-induced and wind stresses at the water surface is about 7%–25% at our experimental conditions. The contribution of rain-induced stress is higher for lower winds and heavier rain conditions. Since the rain-induced stress contributes to the wave growth rather than the damping, this explains partially the smaller damping rate of the present study compared to that measured by Tsimplis and Thorpe (1989).

The vertical momentum flux carried by the rain, M, is defined by $M = \rho WI$ (Manton 1973), where W is the fall velocity of raindrops just before hitting the water surface. In Tsimplis and Thorpe's (1989) experiment, the water drops fall over a distance of 1.25 m, and they estimated the fall velocity of the drops to be 4.5 m s^{-1}. The vertical momentum flux, M, in their experiment is therefore about 0.75 N m^{-2}. For our experimental conditions, the values of M are only between 0.02 and 0.05 N m^{-2} for rain intensities between 35 and 100 mm h^{-1}; these are more than one order of magnitude smaller than that in Tsimplis and Thorpe's experiment. It is reasonable to assume that the mixing strength induced by rain is related to the vertical momentum flux (Manton 1973). With such a great difference in momentum fluxes produced by different rains in the present and Tsimplis and Thorpe's experiments, it is not surprising to see that there is a difference of about 100% in the measured damping coefficients for $2 < f < 3.5$ Hz. Due to the fluctuation in our spectral estimates, it is difficult to see from the present study the effect of rain intensity on the damping coefficients $\Delta(f)$ presented in Fig. 6. Moreover, in the presence of wind, the increase in rain-induced surface stress compensates partially the increase in damping with the rain intensity. In Fig. 7, the ratio of the rms surface displacement with rain to that without rain is shown. Although the data are limited, a trend of increased damping with the rain intensity can still be seen. From the present study, together with the results of Tsimplis and Thorpe, we can conclude that there is an increase in wave damping with the rain intensity. For natural rains, Manton estimated that under "ordinary" conditions ($I = 3.6$ mm h^{-1}), $M = 0.006$ N m^{-2}, and for "violent rain like a cloud burst with some hail" ($I = 43.2$ mm h^{-1}), $M = 0.098$ N m^{-2}. For the present study the simulated rain conditions are better representations for natural rains, at least for simulating the vertical momentum fluxes. Moreover, the present study also simulates the rain-induced surface stress that is absent in Tsimplis and Thorpe's experiment.

b. Comparison of measured damping rates with analytical estimates

Based on the momentum exchange between rain and water waves, Le Mèhautè and Khangaonkar (1990) established a theory to determine the dynamic effect

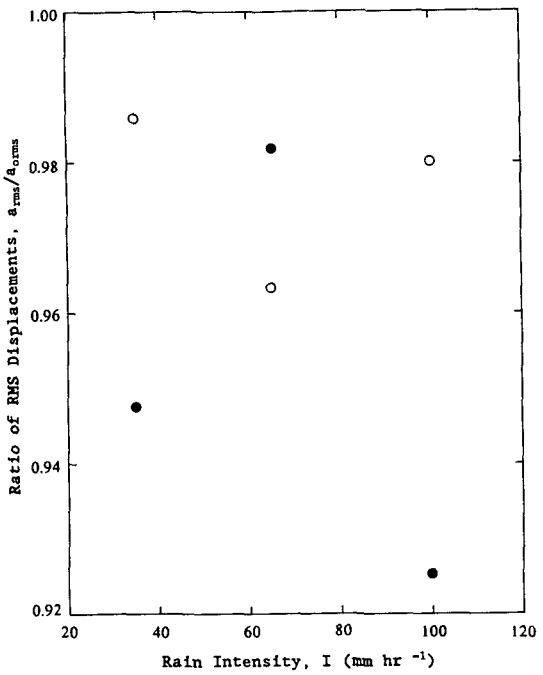

FIG. 7. The ratio of rms surface displacement measured with rain to that without rain at different rain intensities. Measurements are taken at wind velocities of 4.88 (+) and 6.34 (∗) m s^{-1}, respectively.

of intense rain on waves. They considered a uniform rain with drops entering water with speed V_r at a zenith angle α. It was assumed that as soon as a drop reaches the water surface, its mass is entrained by the current in a thin boundary layer and hence is subjected to a change of momentum. It was further assumed that as a result of the rain, the amplitude of the wave varies exponentially with time, and the wave field can be defined as Airy waves. The momentum change as the rain enters the water was then converted to a fluctuating pressure and shear stress acting on the water surface. Following Longuet-Higgins' (1969) approach on the effects of a variable stress on water waves, they obtained a dispersion relationship relating the complex frequency $\sigma\ (=\sigma_r + i\sigma_i)$ to the rain and wave conditions. The imaginary part σ_i corresponds to the temporal wave growth ($\sigma_i > 0$) or wave decay ($\sigma_i < 0$) coefficients such that the amplitude of wave changes from A_0 to A in time t according to

$$A = A_0 \exp(\sigma_i t). \tag{5}$$

The complex dispersion equation cannot be solved analytically. However, Le Mèhautè and Khangaonkar (1990) found numerically that σ_r is not sensitive to rain; in most practical conditions (except when rain is nearly horizontal) and in deep water

$$\sigma_i = \frac{\rho}{\rho_s} Ik\left[\frac{V_r}{2}\left(\frac{k}{g}\right)^{1/2} \sin\alpha - \frac{3}{2}\right], \tag{6}$$

where ρ_s is density of sea water. In the case of vertical rain, Eq. (6) simply reduces to

$$\sigma_i = -\frac{3}{2}\frac{\rho}{\rho_s} Ik. \tag{7}$$

To compare the predicted damping rate with those measured in the present and Tsimplis and Thorpe's (1989) studies, we convert the temporal decay coefficient σ_i to the spatial damping coefficient Δ according to

$$\Delta = \frac{|\sigma_i|}{c}, \tag{8}$$

where c is the phase velocity of waves. In comparing the theory with Tsimplis and Thorpe's results, Eq. (7) is used since the rain is falling vertically in their experiments. To compare the theory with the present study, Eq. (6) is used with V_r and α estimated from the numerical simulation discussed earlier. The comparisons are shown in Fig. 8; the theory is seen to underpredict the damping coefficients by one to two orders. Hence, the momentum exchange may not be the dominant mechanism leading to the damping of surface waves by rain.

Le Mèhautè and Khangaonkar's (1990) theory has considered the most direct effect of rain on waves. The

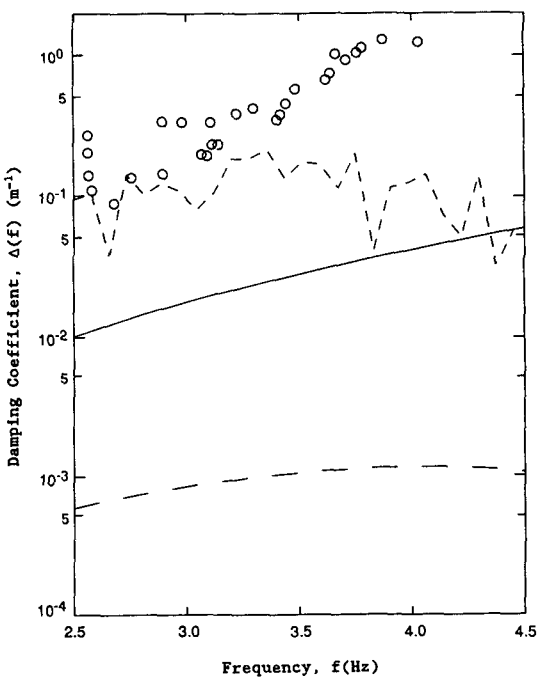

FIG. 8. Comparisons between the measured and predicted damping coefficients. The measurements are from Tsimplis and Thorpe (1989) (open circles) and this study with rain intensity of 65 mm h^{-1} (short-dashed line). The theoretical prediction corresponding to the former measurement is shown as the solid line and the latter as the long-dashed line.

change of momentum of raindrops is converted to a force acting on the water surface as a part of the free surface conditions. However, most of the rain energy may be expended in generating a turbulent mixing layer near the water surface. The enhanced mixing is then interacting with surface waves, leading to their damping; this will be further discussed in the next two sections.

c. *Rain-induced mixed layer*

Long ago, Reynolds (1900) suggested that the attenuation of waves by rain is due to the vertical mixing of the surface water layer, enhanced by the formation of vortex rings introduced by raindrops. Laboratory experiments on the rain-induced mixing (Katsaros and Beuttner 1969; Green and Houk 1979) showed that under various rain conditions, a mixed layer having depth between 5 and 20 cm was formed. Tsimplis and Thorpe (1989) suggested that the effective eddy viscosity within the rain-induced mixed layer, ν_e, could be calculated from an expression similar to the molecular viscosity,

$$\Delta(f) = 4(2\pi f)^5 \nu_e(f)/g^3. \quad (9)$$

Values of ν_e obtained by Tsimplis and Thorpe and from this experiment are shown in Fig. 9. The values of ν_e calculated from Eq. (9) are based on the damping coefficients shown in Fig. 6. Only positive ν_e are shown; the few negative ν_e corresponding to negative damping coefficients measured at low frequencies are not shown. We can see that the intensity of mixing, reflected by the effective eddy viscosity, decreases as the frequency increases. Tsimplis and Thorpe's results show a stronger mixing than the present results; this is due to differences in the rain conditions as discussed earlier. For $2.5 < f < 4$ Hz, an average value of $\nu_e = 2.8 \times 10^{-5}$ m^2 s^{-1} was suggested by them; it is 1.2×10^{-5} m^2 s^{-1} from our results. Both values are significantly higher than the kinematic viscosity of water, which is only about 1×10^{-6} m^2 s^{-1} at 20°C.

d. *Selective damping of gravity waves by rain*

A simple model for evaluating the wave damping by rain due to the enhanced effective eddy viscosity in the rain-induced mixed layer was proposed by Nystuen (1990). He showed that the wave decay due to the enhanced eddy viscosity in the rain-induced mixed layer could be represented by

$$\frac{1}{E}\frac{dE}{dt} = -4k^2[(1 - e^{-2kD})\nu_e + e^{-2kD}\nu], \quad (10)$$

where dE/dt is the temporal rate of change of the spectral density, D the thickness of the rain-induced mixed layer, and ν the kinematic viscosity of water.

Using the values of ν_e obtained by Tsimplis and Thorpe (1989) and this study, that is, 2.8×10^{-5} and 1.2×10^{-5} m^2 s^{-1}, respectively, and taking D as 10 cm (Green and Houk 1979), we calculate the ratio between the e-folding time in the presence of rain to that due to molecular mixing, T_{er}/T_{eo}. The results are plotted against the wavenumber in Fig. 10, showing

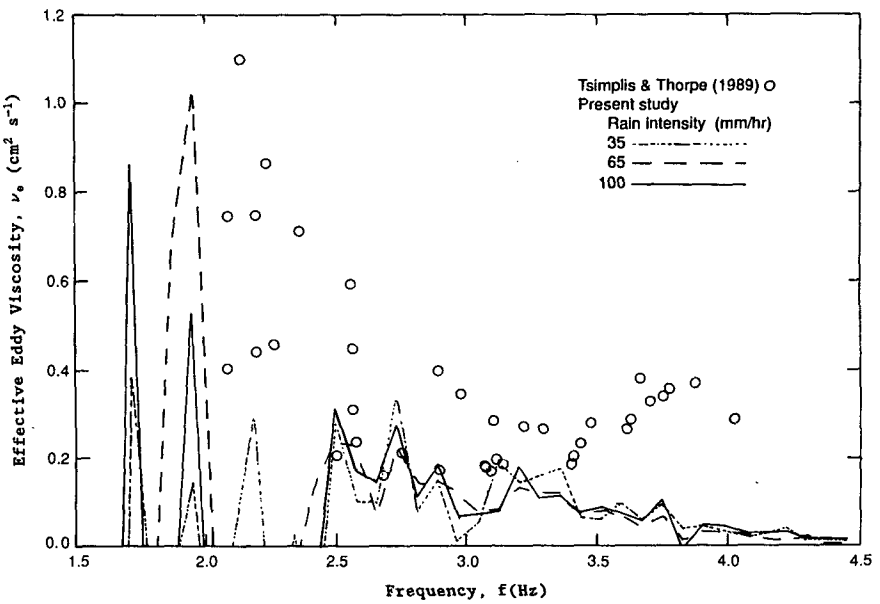

FIG. 9. Comparisons of effective eddy viscosities obtained by Tsimplis and Thorpe (1989) and this study.

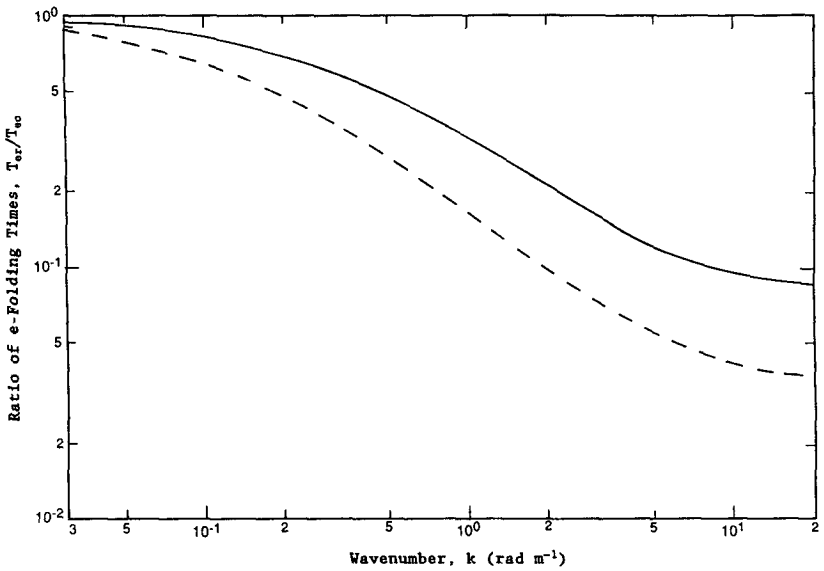

FIG. 10. The ratio of e-folding times in the presence of rain to that by molecular mixing, T_{er}/T_{eo}, at various wavenumbers. The calculation is based on taking the thickness of the rain-induced mixed layer, D = 10 cm, and the effective eddy viscosity, $\nu_e = 1.2 \times 10^{-5}$ (solid line) and 2.8×10^{-5} (dashed line) m^2 s^{-1}, respectively.

clearly that rain has a greater damping effect on shorter rather than longer waves. Based on $\nu_e = 1.2 \times 10^{-5}$ m^2 s^{-1}, T_{er}/T_{eo} decreases gradually as the wavenumber increases. For k = 21 rad m^{-1}, that is, the wavelength equals 30 cm, as pointed out by Nystuen (1990), which is important for SAR (L-Band) measurements, T_{er}/T_{eo} is about 0.085, indicating that the waves in the presence of rain decay 12 times faster than in the absence of rain. This clearly illustrates the rain has significant effects on signals from remote sensors. The effect of rain on surface waves, however, diminishes as wavenumber decreases; when k approaches 0.03 rad m^{-1}, that is, wavelength equals 200 m, T_{er}/T_{eo} approaches 0.93.

e. *Comparison of measured rain-generated ripples with analytical estimates*

Recently, Le Mèhautè (1988) quantified analytically waves generated by the impact of individual water drops on an initially quiescent water body. Waves in the capillary–gravity regime are generated. Around the minimum group velocity, waves observed at any distance away from the impact point are the linear superposition of two wave components: the super-k_m ($k > k_m$) and sub-k_m ($k < k_m$) wave components, where k_m is the wavenumber corresponding to the minimum group velocity. Most waves observed are in a narrow band around k_m. At a short distance from the impact point, the super-k_m components have a relatively large amplitude and hide the sub-k_m components. However, at large distances, the super-k_m components are damped rapidly and only the sub-k_m components are still visible.

Our experiments are performed with filtered tap water; taking the surface tension of 74 dyn cm^{-1}, the minimum group velocity is 17.9 cm s^{-1} and the frequency f_m corresponding to k_m is 6.41 Hz. Normalized wave amplitudes of the sub-k_m and super-k_m components versus time at distances of 30, 60, and 120 cm away from the drop were presented by Le Mèhautè in his Fig. 1; the amplitude of super-k_m components at a distance of 30 cm from the point of impact is seen to be much greater than that of sub-k_m components. At a distance of 60 cm away, the amplitudes of these two components are comparable in magnitude. In our experiments, the ripple structures were measured at a distance of 18 cm from the downwind edge of the 100-cm-long simulated rain region. For half of the simulated rain region, the distance between the raindrops and the measuring location is less than 60 cm, hence ripples that reach the measuring point are dominated by the super-k_m components even when there is no wind. In the presence of wind, the rain-generated ripples are convected by long waves and surface drift currents to the measuring location. Hence, we expect that even for ripples generated at the farthest end from the measuring point (118 cm), the super-k_m components are not damped by the time they reach the location of measurements. Such a dominance of rain-generated ripples with the super-k_m component can also be seen from our measurements, as rain-generated ripples have

frequencies higher than 10 Hz, which is higher than f_m. Moreover, if the Doppler effect is corrected, the frequency of rain-generated ripples is found to be higher than about 7 Hz, very close to the predicted f_m of 6.41 Hz according to Le Mèhautè's theory. Of course, rain-generated ripples of lower frequencies (in the sub-k_m regime) are present. Their presence, however, is simply masked by the wind-generated ripples.

f. Influence of rain-generated ripples to radar signals

The effects of rain on radar signals were studied by Moore et al. (1979) and Bliven and Norcross (1988) in wind-wave tanks with artificial rains. Moore et al. found that with a FM radar operating at 14 GHz (2.2-cm wavelength) and incidence angle of 40°, the radar cross section increased with the rain intensity under light winds and produced little changes under heavy winds. Similar results were found by Bliven and Norcross with a radar operating at 36 GHz (8.3-mm wavelength) and pointing upwind at an incidence angle of 60°. In natural rain conditions, Hansen (1984) operated an X-band radar (3.2-cm wavelength) near grazing incidence. He found that under initially calm sea and wind conditions, the radar sea return is greatly increased due to the rain. However, for rougher initial sea and wind conditions, the change in the return signals is much less dramatic.

According to the Bragg scattering, the radar sea returns are from surface waves of Bragg wavelength λ satisfying

$$\lambda = \lambda_r/(2 \sin\theta), \tag{11}$$

where λ_r is the radar wavelength and θ is the angle of incidence. For Moore et al.'s measurements, the Bragg wavelength is about 1.67 cm and the corresponding values for Bliven and Norcross' and Hansen's measurement are, respectively, 0.48 and 1.6 cm. Our results indicate that rain is effective in generating ripples of frequencies higher than about 10 Hz; it corresponds to wavelengths less than about 3.8 cm following the removal of Doppler shifts. Moreover, our results indicate that the ripple structures are most affected by rain under low winds (3.41 and 4.88 m s^{-1}); at high wind (6.34 m s^{-1}), the effect of rain-generated ripples is no longer important. Of course, under different wind velocities, the structure on the part of rain-generated ripples should not change significantly. It is the increase of wind-generated ripples, which eventually mask the presence of rain-generated ripples.

5. Conclusions

We have shown experimentally that rain has effects on wind waves at two different scales. For the low-frequency waves, they are attenuated by the rain, and most of the damping occurs within a narrow frequency band of 2–5 Hz. Together with the measurements of Tsimplis and Thorpe (1989), it is shown that the damping rate increases with rain intensity. Comparisons of the damping coefficients measured by Tsimplis and Thorpe and in the present study with those predicted by Le Mèhautè and Khangaonkar's (1990) theory revealed that momentum exchange between the rain and surface waves may not be the dominant mechanism of wave damping. To explain the damping in terms of the mixing generated by rain near the water surface, an effective eddy viscosity of 1.2×10^{-5} m^2 s^{-1} is found. It is also found that the rain has greater damping effects on shorter than longer gravity waves. For waves with wavelength of 30 cm, the damping rate in the presence of rain is 12 times that without rain; and for waves longer than 200 m, the damping effect of rain is not important. For ripples, the presence of rain at low-wind conditions can drastically enhance the slope spectral density for frequencies between 10 and 100 Hz. At high wind conditions, however, the structure of ripples is dominated by the wind and there is no observable influence by the rain. Our measured changes in rain-generated ripples with the changes of wind conditions can explain the observed changes in radar sea returns under rain.

Further studies are necessary to explain the attenuation of waves by rain, especially on the mechanisms that lead to damping. It is suggested that the turbulence structure at the near water surface be measured simultaneously with changes in the waves. Hence, direct correlation between the mixing induced by rain and the resulted damping can be sought. To better understand the effect of rain on radar returns, simultaneous measurements on changes in radar return signals and surface ripple structures are also suggested.

Acknowledgments. We are very grateful for the sponsorship of our research provided by the Remote Sensing Program, Office of Naval Research, under contract N00014-89-J-3226; the Physical Oceanography Program, National Science Foundation, under Contract OCE-8716519; and the Ocean Dynamics Program, National Aeronautics and Space Administration, under Contract NAGW-2981.

REFERENCES

Banner, M. L., 1990: Equilibrium spectra of wind waves. *J. Phys. Oceanogr.*, **20**, 966–984.

Blackman, R. B., and J. W. Tukey, 1959: *The Measurement of Power Spectra.* Dover, 190 pp.

Bliven, L. F., and G. Norcross, 1988: Effects of rainfall on scatterometer derived wind speeds. *Proc. IGARSS '88 Symp.*, Edinburg, 565–566.

Caldwell, D. R., and W. P. Elliott, 1971: Surface stress produced by rainfall. *J. Phys. Oceanogr.*, **1**, 145–148.

——, and ——, 1972: The effect of rainfall on the wind in the surface layer. *Bound.-Layer Meteor.*, **3**, 146–151.

Cataneo, R., and G. E. Stout, 1968: Raindrop-size distributions in humid continental climates and associated rainfall rate—Radar reflectivity relationships. *J. Appl. Meteor.*, **7**, 901–907.

Chapman, D. S., and P. R. Critchlow, 1967: Formation of vortex rings from falling drops. *J. Fluid Mech.*, **29**, 77–185.

Green, T., and D. F. Houk, 1979: The mixing of rain with near-surface water. *J. Fluid Mech.*, **90**, 569–588.

Haimbach, S. P., 1985: Development of slope spectra of the wind-disturbed water surface. Ph.D. dissertation, College of Marine Studies, University of Delaware, 184 pp.

Hansen, J. P., 1984: High resolution radar backscatter from a rain disturbed sea surface. *Proc. Int. Symp. on Noise and Clutter Rejection in Radars and Imaging Sensors*, Tokyo, 123–128.

Houk, D. F., and T. Green, 1976: A note on surface waves due to rain. *J. Geophys. Res.*, **81**, 4482–4484.

Katsaros, K., and K. J. Buettner, 1969: Influence of rainfall on temperature and salinity of the ocean surface. *J. Appl. Meteor.*, **8**, 15–18.

Kilgore, E. G., and J. A. Day, 1963: Energy dissipation of water drops striking an undisturbed water surface. *Tellus*, **15**, 367–369.

Le Mèhautè, B., 1988: Gravity-capillary rings generated by water drops. *J. Fluid Mech.*, **197**, 415–427.

——, and T. Khangaonkar, 1990: Dynamic interaction of intense rain with water waves. *J. Phys. Oceanogr.*, **20**, 1805–1812.

Long, S. R., and N. E. Huang, 1976: On the variation and growth of wave-slope spectra in the capillary-gravity range with increasing wind. *J. Fluid Mech.*, **77**, 209–228.

Longuet-Higgins, M. S., 1969: Action of a variable stress at the surface of water waves. *Phys. Fluids*, **12**, 734–740.

Manton, M. J., 1973: On the attenuation of sea waves by rain. *Geophys. Fluid Dyn.*, **5**, 249–260.

Moore, R. K., Y. S. Yu, A. K. Fung, D. Kaneko, G. J. Dome, and R. E. Werp, 1979: Preliminary study of rain effects on radar scattering from water surfaces. *IEEE J. Oceanic Eng.*, **OE-4**, 31–32.

Nystuen, J. A., 1990: A note on the attenuation of surface gravity waves by rainfall. *J. Geophys. Res.*, **95**, 18 353–18 355.

Phillips, O. M., 1985: Spectral and statistical properties of the equilibrium range in wind-generated gravity waves. *J. Fluid Mech.*, **156**, 505–531.

Raudkivi, A. J., 1976: *Loose Boundary Hydraulics*. 2nd ed., Pergamon, 397 pp.

Reynolds, O., 1900: On the action of rain to calm the sea. *Papers on Mechanical and Physical Subjects, Vol. I*, Cambridge University Press, 86–88.

Shemdin, O. H., 1972: Wind-generated current and phase speed of wind waves. *J. Phys. Oceanogr.*, **2**, 411–419.

Siscoe, G. L., and Z. Levin, 1971: Water-drop–surface-wave interactions. *J. Geophys. Res.*, **76**, 5112–5116.

Toba, Y., 1973: Local balance in the air–sea boundary processes III. On the spectrum of wind waves. *J. Oceanogr. Soc. Japan*, **29**, 209–220.

Tsimplis, M., and S. A. Thorpe, 1989: Wave damping by rain. *Nature*, **342**, 893–895.

Wang, J., and J. Wu, 1987: Effects of near-bottom return flows on wind-induced currents. *J. Phys. Oceanogr.*, **17**, 2263–2271.

——, and C.-S. Chern, 1988: Observations on wave-turbulence interactions. Abstract. *Eos, Trans., Amer. Geophys. Union*, **69**, 1264.

Willis, P. T., and P. Tattelman, 1989: Drop size distributions associated with intense rainfall. *J. Appl. Meteor.*, **28**, 3–15.

Wright, J. W., and W. C. Keller, 1971: Doppler spectra in microwave scattering from wind waves. *Phys. Fluids*, **14**, 466–474.

Wu, J., 1975: Wind-induced drift currents. *J. Fluid Mech.*, **68**, 49–70.